DETECTION AND MONITORING OF FOREST FIRES IN CHINA THROUGH THE ENVISAT-AATSR SENSOR

A. Calle, J.A. Sanz, C. Moclan, A. Romo, J.L. Casanova

Remote Sensing Laboratory of University of Valladolid ,LATUV
Dpt. Applied Physics, Faculty of Sciences, 47071-Valladolid (Spain)
E-mail: abel@latuv.uva.es

The detection of forest fires through the ATSR sensor on board the ERS European satellites has been widely studied and analyzed on European and African territories. Putting the ENVISAT satellite in orbit has allowed us to bring the AATSR sensor (*Advanced Along Track Scaning Radiometer*) into operation, whose spectral and radiometric capacities are very advanced with respect to its predecessor. This sensor has raised high expectations in relation with the statistical global results of fire occurrence. However, the existing algorithm parameters need to be revised and modified for new territories that have different forest cover characteristics from the ones that have already been studied and validated.
In this paper, we present an analysis on fires occurred on the north-east of China during 2002 and 2003 in order to adjust the detection algorithms to the new environmental conditions.
The Remote Sensing Laboratory of the University of Valladolid is leader in the forest fires group in the DRAGON project, which is financed by the ESA in collaboration with the Science and Technology Ministry of the Popular Republic of China. The present paper is part of this work.

Introduction

The use of remote sensing techniques for the study of forest fires is a subject that started already several years ago and whose possibilities have been increasing as new sensors were incorporated into earth observation international programmes and new goals were reached based on the improved techniques that have been introduced. In order to place this subject of study in its appropriate context, it must be pointed out that fire detection with an aim to create alarms that facilitate a rapid extinction is a necessity that hasn't been resolved yet. And it won't be solved until the geostationary satellites show their capacity to detect small fires and prove themselves useful to generate early alarm warnings, which seems pretty difficult given the difficulty in having high spatial resolution thermal sensors. In this sense, simulations have been carried out in order to establish the minimum detectable area according to the temperature on GOES and MSG [1], which are the most capable geostationary sensors to carry out this task. In the MSG's case, and on our latitudes, in order to detect a fire of 600 K a flame size larger than 1.5 ha is needed and this without including the effects of atmospheric attenuation. However, several research groups are already using MSG images to carry out the detection of hot-spots in real time and improve the detection algorithms as a larger number of cases are available. These improvements are aimed at the eradication of false alarms rather than at the perfection of the detection itself. On the other hand, the attempt to establish a system of early fire detection by means of polar satellites, which would solve the problem of spatial resolution, has already been considered in the well-known FUEGO project, that is currently being modified in its original definition through another initiative led by the ESA known as FUEGOSAT, which is being developed at this moment. The most relevant conclusion with respect to the current usefulness of fire detection through spatial sensors is that up until now, it has been useful mainly for the elaboration of fire occurrence maps and the obtaining of statistical results [2].

Up until now, the polar satellites most widely used for detection tasks have been the NOAA-AVHRR [3], the EOS-MODIS [4] and the European sensor ATSR-2. In March 2002, the ESA put into orbit the ENVISAT satellite allowing us to put the advanced sensor AATSR (*Advanced Along Track Scanning Radiometer*) into operation. As is already known, this satellite has two different ways of observation: the nadir vision and the observation with a sloping angle of 55º in front of the sub-satellite point at a distance of approximately 1000 km above the ground. This observation is used for atmospheric correction processes taking into account that it is carried out at an interval of 150 seconds later than the former one. With respect to the spectral characteristics, AATSR has 7 bands centered in 0.56, 0.66, 0.87, 1.61, 3.70, 10.85 and 12 μm respectively. The radiometric resolution these bands provide is quantified in 12 bits. Table 1 shows the radiometric characteristics of these bands. It must be pointed out that although this sensor's main goal is the study and establishment of the sea temperature, its characteristics for fire observation, detection and monitoring have already been made clear by its predecessors ATSR-1 and ATSR-2 [5].

Table 1. Radiometric characteristics of AATSR sensor.

Channel	Nominal working range	NE delta(T) at 270 K	S/N at 0.5% albedo
0.55 μm	0 - 50 mW cm^{-2} μm^{-1} sr^{-1}	N/A	20:1
0.66 μm	0 - 45 mW cm^{-2} μm^{-1} sr^{-1}	N/A	20:1
0.87 μm	0 – 30 mW cm^{-2} μm^{-1} sr^{-1}	N/A	20:1
1.6 μm	0 – 7 mW cm^{-2} μm^{-1} sr^{-1}	N/A	20:1
3.7 μm	0 - 311 K	0.08 K	N/A
11 μm	200 - 321 K	0.05 K	N/A
12 μm	200 - 318 K	0.05 K	N/A

The present work has a double aim. On the one hand, to carry out an exhaustive analysis of the AATSR sensor's response to the variation of different parameters which are difficult to quantify in real time and for each point in the territory according to the potential characteristics that the fire observed has. On the other hand, to apply the detection and monitoring techniques to fires that occurred in the northern regions of China, where the environmental conditions are different from the ones existing in Mediterranean Europe.

Physics Principles: detection and monitoring

Hot-spots detection

The detection has been developed through different algorithms that can be schematically classified into algorithms based on fixed thresholds [6] and contextual algorithms [7], whose parameters have been adapted to the different zones of study. Both types of algorithms have advantages and disadvantages and their application will depend on the type of sensors to which they are going to be applied. The detection algorithms based on fixed thresholds, also called multi-channel, are based on the establishment of minimum temperature values in different spectral bands from which the detection is established. The most common scheme is to consider that a pixel is affected by a fire when the following conditions are fulfilled simultaneously:

$$\begin{cases} T_{MIR} > V_{MIR} \\ T_{MIR} - T_{TIR} > V_{DIF} \\ T_{TIR} > V_{TIR} \\ R_{NIR} < V_{NIR} \end{cases},$$

where MIR and TIR refer to the spectral bands of the 3.7 μm and 11 μm regions respectively. In the former test, the first two conditions are the ones that carry out the detection of hot-spots strictly speaking according to the physic principles previously stated. The T_{MIR} test is for fire detection and the T_{MIR}-T_{TIR} test is to carry out the differentiation between the fire, which has high values in the MIR, and the hot surfaces which have high values both in the MIR and TIR. The T_{TIR} test is a cloud filter to apply the test to images in which the cloud cover has not been eradicated through other means. The R_{NIR} test is to filter the reflectance in sun-glint situations that are responsible for the appearance of false alarms. The threshold values established are varied. They depend on the algorithm and, above all, on the geographic area due to the influence that the temperature can have on the environment. Thus, normally low surface temperature values use lower MIR threshold values without the appearance of false alarms. Concretely, to mention an American and a European algorithm both operating on NOAA-AVHRR, we will speak about the CCSR used by the *Canadian Center of Remote Sensing* [8] and the ESA used by the *European Space Agency* [9] respectively. The CCSR is a valid algorithm on a regional scale and it uses the threshold values V_{MIR}=315 K, V_{DIF}=14 K, V_{TIR}=260 K and V_{NIR}=22%, whereas the ESA algorithm is valid both on a global and on a regional scale and takes the values V_{MIR}=320 K, V_{DIF}=15 K, V_{TIR}=245 K and V_{NIR}=25%. Both will be compared in the results section. To provide some quantitative values, the experience on the AVHRR has proved that a MIR temperature threshold of 320 K is appropriate for the detection of fires in tropical forests, whereas in boreal forests a value of 310 K would be better.

The disadvantage of the algorithms based on fixed thresholds is that the values established depend on the zone of study and their environmental temperatures. In order to avoid this dependence, contextual algorithms can be used. They are based on the obtaining of threshold values carrying out a statistical analysis of the environment, which is analyzed in a matrix with a size of $N \times N$ pixels, being N an odd value that depends on the sensor to which it is applied. Two representative examples are the IGBP algorithm (*International Geosphere Biosphere Program)* [10], and an adaptation of the current algorithm on MODIS [11]. Contextual algorithms have the advantage of making the detection process independent from the season and the zone analyzed, since the thresholds are obtained by means of an statistical analysis of the environment. However, they have a serious drawback when they are applied to images in which the clouds have not been filtered since cloud edges cause false alarms.

Fire monitoring

With respect to fire monitoring, a more realistic scheme derived from Dozier's methodology is the one suggested by *Giglio & Kendall* [12]. This scheme modifies the former one by including terms of emissivity, atmospheric effects and sun reflection in the radiance equation of the MIR band. The following are the modified equations of Dozier:

$$\begin{cases} L_{MIR} = \tau_{MIR} \cdot p \cdot B(\lambda_{MIR}, T_f) + (1-p) \cdot L_{surf,MIR} + p \cdot L_{atm,MIR} \\ L_{TIR} = \tau_{TIR} \cdot p \cdot B(\lambda_{TIR}, T_f) + (1-p) \cdot L_{surf,TIR} + p \cdot L_{atm,TIR} \end{cases}, \; 0 < p < 1 \;,$$

where $L_{atm,MIR}$ and $L_{atm,TIR}$ are the radiances emitted by the atmosphere to the sensor in the MIR and TIR bands respectively. These terms are worthless with respect to the radiances emitted by the surface, $L_{surf,MIR}$ and $L_{surf,TIR}$, and can be disregarded. τ is the atmosphere's spectral transmittance. The difference in these equations with respect to the original ones lies in the intervention of the radiances of the surrounding pixels instead of the temperature and finally, although they are taken into account, the surface's emissivity and temperature are not usually known explicitly. The techniques mentioned for the obtaining of fire parameters imply some difficulties related to the errors that are made. In the first place, they are not analytic equations so that their solution must be found by means of numerical calculation techniques. However, it must be said that their solution comes, in the end, from a convergent system. Other important sources of errors have their origin in different magnitudes that have been analyzed by *Giglio & Kendall* [12].

Analysis of AATSR sensor

The obtaining of results through the application of the bi-channel equations is a very delicate task since, as the solution is not obtained analytically, it is necessary to apply procedures of numerical calculation. On the other hand, the application of these equations requires the knowledge of both atmospheric and surface data, which are very difficult to quantify through remote sensing and in the real time in which these equations are carried out. This is the case of the atmospheric transmittance and earth parameters such as the surface emissivity and the surface temperature. It must be noticed that the fire has been considered as a blackbody, but not so the non-affected surface in the pixel, which contributes with the radiance term. On the other hand, the variation of all these parameters must be carried out for each sensor in particular since, in the end, and at the sensor's level, the apparent temperature provided will be filtered by the spectral response function.

In this section, we will tackle the analysis of the AATSR sensor according to the response obtained coming from pixels where there is a fire and quantifying the effects produced by the variation of the parameters mentioned in order to see whether taking approximations in the calculation method is justified or not.

Spectral response function of MIR AATSR

The main spectral band involved in fire detection and monitoring is the one centered in 3.75 μm. This response function has a width equivalent to 0.35 μm. In order to analyze the atmospheric and spectral effects to which it is subjected, fig.1 shows a comparison of the functions in the MIR bands of the AVHRR, MODIS, BIRD and AATSR sensors, as well as the spectral transmittance. As can be observed, the AATSR function is more similar to the AVHRR one, as much in width as in center and form. It is narrower than BIRD's and this makes it possible to appear very well centered in the atmospheric window in this part of the spectrum. The largest difference is with respect to the MODIS function, which is much narrower. The MODIS function is displaced towards higher wavelengths, which implies a minor disturbance with respect to water vapor absorption and that it receives up to 40% less sun reflection. This is a very important datum in relation to the generation of false alarms and for a better accuracy in the calculation of fire parameters.

Dependence on Surface Emissivity

The bi-spectral equations proposed by *Giglio & Kendall* [12], mentioned above, set out the radiance emission of a pixel divided, in a simplified way, into fire and background. In this last case, the radiance emitted depends on the surface emissivity, which moves further away from the behavior of a blackbody than in the case of the fire. In order to know how the variation in the surface emissivity affects the brightness temperature provided by the final sensors for different temperatures and fire sizes, different simulations have been carried out through the MODTRAN code using, also, the spectral response function of the 3.75 and 11 μm bands of the AATSR sensor.

In order to carry out this analysis, fire temperatures in the interval [350, 1100 K] were taken with an increase of 10 K and with fractions of pixel affected by the fire in the interval [0,1]. Special attention was paid to small values, where increases of 0.0001 were applied. With this scheme, the brightness temperatures that the AATSR sensor should provide in the bands involved in detection were established for standard atmospheric pro-

files. Fig.2 shows a representative result for the qualitative discussion. In it, a value of 300 K has been used for the temperature of the surface non-affected by the fire. The figure represents the potential fire temperature values on the abscissas, the brightness temperature of band 3.7 on the first ordinates axis and, on the second ordinates axis, the brightness temperature difference in that band from considering the surface as a black body and considering an emissivity body with a value of 0.95. Four different fractions of a pixel affected by the fire are represented: 0.0001, 0.001, 0.015, and 0,02. In the same figure, we can observe the sensor's saturation level, which means that only the detection could be carried out, but never the establishment of the fire parameters.

As was expected, different emissivity values affect more strongly the conditions in the pixels which are little affected by the fire, for which the ground contribution and lower fire temperature values are more important. Thus, a 100 m^2 fire at a temperature of 1000 K surrounded by a surface at 300 K is just in the saturation conditions and the difference from considering the emissivity value as 1 or 0.95 in that surface is little more than half a K in the brightness temperature. A fire of 8000 m^2 at a temperature of 450 K would saturate the pixel.

Logically, this temperature difference is larger as surfaces with lower emissivity values are considered. Table 2 shows the maximum differences in brightness temperatures found in the MIR band, for the burning fractions of the pixel mentioned above and for emissivity values in the interval [0.95, 0.8]. These maximum differences correspond to the fires where the lowest temperatures were considered, 350 K in this case. On the other hand, this difference decreases as the surface taken by the fire increases so that this table is representative of the maximum errors committed. Let's also remember that forest fire observation is carried out on forested lands so that the most frequent real emissivity values will be superior to 0.95. Thus, maximum differences of 4.8 K have been found when considering the emissivity as 0.8 and for burning pixel fractions of 10^{-4}.

Table 2. Differences in MIR temperature (K) from considering Black Body and real surface, for different fire fraction values.

	Fraction pixel with fire			
Emissivity	0.0001	0.001	0.015	0.02
0.95	1.1	1.1	1.0	1.0
0.9	2.3	2.3	2.1	2.1
0.8	4.8	4.8	4.4	4.3

Dependence on atmospheric transmittance

Another parameter that intervenes in the bi-spectral equations and that cannot be established with accuracy is the atmospheric transmittance and, implicitly, the different types of aerosols which are present at the moment of the observation. In order to carry out this analysis, we have considered our goal to find out what the brightness temperature difference is obtained at the sensor level in bands 3.7 and 11 μm for different fire temperatures and different occupied fractions as a consequence of applying different atmospheric profiles: summer in middle latitudes, winter in middle latitudes, US-standard 1976 and tropical. For each of them, two types of aerosols have been simulated, one with a weak visibility attenuation of 23 km and the other one, stronger, with a visibility of 5 km.

Fig.3 summarizes the most representative results. In it, for each of the bands 3.7 and 11μm, the brightness temperature difference at the sensor level is represented according to the existing fire temperature as a consequence of considering different atmospheric situations whose transmittance is shown in detail. These results have been obtained for a surface temperature of around 300 K and with a high value for the pixel's fraction, 0.04 equivalent to $4 \cdot 10^4$ m^2.

The differences increase as the fire temperature increases. In the case of the MIR band, and close to saturation conditions, there are differences of 2K in the transmittance interval [0.89=middle latitude winter, vis. 23 km, 0.74=middle latitude summer, vis. 5 km (in both cases rural aerosols are considered)]. In the case of the TIR band, there are higher differences, finding values close to 10 K for fire temperatures of 700 K and in the atmospheric transmittance interval [0.92, 0.63], which represent the profiles mentioned above. On the other hand, this extreme situation would never be considered for the establishment of fire parameters due to the saturation of band MIR. For a fraction of 0.04 covered by a fire, this saturation would have taken place at around 400K. In these conditions, the brightness temperature differences found in the TIR band would have been approximately 3.5 K.

Dependence on background temperature

The last variable that intervenes in the bi-spectral equations, and that is difficult to quantify, is the temperature of the non-burning surface of the pixel affected by the fire. In order to establish it, we can consider this value as the mean of the surface temperature values of the surrounding pixels which are not on fire. This value, thus determined, is an approximation and becomes less accurate as the dispersion of the values used for its calculation increases.

In fig.4, representative graphs of the simulations carried out are presented. The brightness temperature values at the sensor level are shown in the MIR band, which is the one most affected by this variation. A fire surface of 100 m^2 has been considered in part a) and of $2 \cdot 10^4$ m^2 in part b). The fire temperature is represented in the abscissas axis and in the graph, the surface temperature values are shown in the interval [290, 300]. As is evident, the largest differences are obtained for the smallest burning fraction of the pixel due to the higher contribution of the surface. The differences are also larger for lower fire temperatures. In any case, we can observe that a variation of 10 K in the surface implies less than 10 K in the temperature obtained by the sensor. The graphs also show the AATSR sensor's saturation line.

Application: Fire detection and monitoring in China

Next, we will present some results obtained in ENVISAT-AATSR images on Chinese territory. All the results presented have been provided by means of an interactive study of the cases that were more likely to be real fires. Thus, we have tried to obtain the representative characteristics so that automated analyses can be carried out later on.

Zone and period of study

The AATSR sensor images have been used for the analysis of forest fires in the northern and eastern regions of China. These regions are the ones framed in fig.5. The zone of study is delimited by the geographic coordinates of the interval: Longitude [127º-131º], Latitude [48º-51ºN]. The analysis was carried out during the months of April, May, June, July and August corresponding to the year 2003 with a total of up to 49 scenes analyzed, although no fires were located in all of them.

Before providing the numerical values relative to the detection and monitoring processes, it must be pointed out that the fires were not found uniformly spread out throughout this period of analysis, even if this was the most sensitive period for fires according to the country's authorities. Thus, a larger number of fires were found during the month of April, followed by May, whereas the number decreased for the rest of the months. Besides, most of the cases were found in night images, although this datum might be influenced by the fact that fires are much more reliable at night, when the sun's contribution does not exist.

Fire detection results

The goal in the detection phase was to search for the thermal conditions in which fires are found in this zone. As seen in the section of Physics Principles, the detection algorithms most successfully applied to the precedent sensor, ATSR-2, were the ones based on thresholds applied to the 3.7 and 11 μm bands and their difference. However, the values suggested by *Arino et al.* [9] of 308 K for the MIR band (World Fire Atlas using AATSR-2), were not appropriate for this zone. Table 3 shows the statistics obtained in the present analysis.

Table 3.

Channel	DIURNAL CONDITIONS	NIGHT CONDITIONS
BRIG. TEMP. 3.7 μM	**310 K**	**305 K**
BRIG. TEMP. 11.0 μM	**286 K**	**274 K**
DIFFERENCE 3.7-11.0 μM	**24 K**	**33 K**
REFLECTANCE 0.87 μM	**12%**	**-----**
REFLECTANCE 0.67 μM	**7%**	**-----**

The statistics of the thermal values were analyzed according to the temperature in bands 3.7 and 11 and the difference between them, distinguishing between night images and diurnal images, always on non-saturated pixels, as is logical. Besides, for diurnal images, the reflectance in bands 0.87 and 0.67 were also analyzed with a view to using them for the filtering of false alarms in the automation of processes.

With respect to the band MIR, a threshold of 310 K was found valid during the day and of 305 K during the night. The difference between both values lies in the contribution of the sun's radiation in the former ones. The most relevant values correspond to the TIR band, whose representative values were 286 K in diurnal situations, and 274 K at night. It is very important to highlight the fact that the highest percentage of fires analyzed was concentrated in the month of April, which explains the low values detected in this zone of the spectrum and for these latitudes. On the other hand, and with respect to the characteristic values of the difference, the mean in pixels with fire was 24 K during the day, and 33 K during the night, which was undoubtedly caused by the really low values of the surface temperature. Finally, the analysis of the reflectance in the diurnal images showed representative values of 12% of pixels with fire in the 0.87μm region and of 7% in the 0.67 μm region. These values were used to filter points that could present sun-glint

situations and high signal values in the MIR; these values are more in accordance with the ones found in Mediterranean Europe.

Fire monitoring results

Once the detection process has been carried out, the establishment of the fire parameters was done automatically on the pixels affected by applying the methodology described in section "Fire monitoring".

The monitoring phase was established through two processing levels: the pixel level and the cluster level. By cluster, it is understood a group of affected, neighboring pixels. The first level consists of the establishment of the fire temperature and the fire's radiative energy. It must be taken into account that the power generated by the fire has three extinction processes: power transmitted by the heating-up of the ground, the power freed by convection processes and the radiated power. The latter one is the one calculated through the parameters accessible to the satellite. Fig.6 shows one of the examples analyzed, where the original scene processed, the fires detected and the analysis of the fire temperature and the fire radiated in MWatts can be observed.

With respect to the analysis at a cluster level, image at fig.6 shows a mask with the clusters detected in our process, enumerated for the obtaining of the cluster's parameters that will be explained below. The figure shows the average temperature values for each cluster. This temperature has been obtained through the mean of the temperature values in each pixel in the cluster, considered by the area occupied by the fire. Finally, the figure shows the power radiated for all clusters as the sum of the powers in each of the pixels that make up the cluster. This parameter is related to the fire's destructive power and, consequently, to the difficulty in the subsequent generation of the zone.

The information obtained for each of the clusters is summarized in the following list for the ones enumerated as 27, 28 and 29.

#Cluster Avg temp (min, max) Area of fire (min, max) Cluster Number coordinates
fire m2 Intensity of pixels

Cluster 27: Tf=683.0K (683, 683)K; Area=0.1 ha.; (802, 802); I=10 MW; N=1; x=294.752 y=178.562
Cluster 28: Tf=641.7K (591,1038)K; Area=0.6 ha.; (60, 2160); I=56 MW; N=5; x=291.778 y=176.583
Cluster 29: Tf=590.0K (590, 590)K; Area=0.2 ha.; (1602, 1602); I=11 MW; N=1; x=288.803 y=176.583

The parameters listed are: number of the cluster corresponding to the mask code in order to be identified, fire temperature averaged and considered by the area occupied by the fire (in brackets, the minimum and maximum fire temperature found in the group of pixels), total area occupied by the fire in that cluster (in brackets, the minimum and maximum found in individual pixels in m^2), the total power radiated by the cluster, the number of pixels affected in the cluster and, finally, the central co-ordinates of the cluster.

Conclusions

Two outstanding parts have been differentiated in this work, both of them referring to the ENVISAT-AATSR sensor:

First, an exhaustive analysis has been carried out on the dependence that certain magnitudes related with the pixels where there is fire present and the magnitudes that provide for the final sensor's measurement. The usefulness of this analysis is to show the sensor's characteristics to obtain fire parameters, as well as its limitations in respect with the saturation of the 3.7μm band. As has been seen, the fact that the atmospheric conditions are not known and are substituted by standard situations, or the fact that the emissivity and the ground temperature are not known either, does not imply strong variations in the brightness temperature measured by the sensor. However, the sensor's low saturation level makes the observation and analysis of fires with high-temperatures or with large fractions of the affected pixel tremendously difficult.

The second part of this work was the application of the methodology at a sub-pixel level to the AATSR sensor for Chinese scenarios. The values found in the temperatures of band 11 μm differ notably from the conditions found in Mediterranean Europe. The difference between bands 3.7 and 11 is the first argument to be introduced in automated detection processes.

References

1. *Prins E., Schmetz J.* Diurnal fire active detection using a suite of International geostationary satellites. GOFC Forest Fire Monitoring and Mapping Workshop, JRC, Ispra, 1999.

2. *Prins E.M., Menzel W.P.* Geostationary satellite detection of biomas burning in South America // Int. J. Rem. Sensing, 1992, Vol.13, P.2783-2789.
3. *Li Z., Kaufman Y.J., Ichoku C., Fraser R., Trishchenkp A., Giglio L., Jin J., Yu X.* A review of AVHRR-based active fire detection algorithms: Principles, limitations and recommendations in Global and Regional vegetation fire monitoring from space: Planning a coordinated international effort, 2001, SPB Academic Publishing, The Hague, Netherlands, P.199-225.
4. *Giglio L., Justice C.O.* Effect of wavelength selection on characterization of fire size and temperature // Int. J. Remote Sensing, 2003, Vol.24, P.3515-3520.
5. *Arino O., Mellinote J.M.* The 1993 Africa fire map // International Journal of Remote Sensing, 1998, Vol.19, P.2019-2023.
6. *Kaufman Y.J., Tucker C.J., Fung I.* Remote sensing of biomass burning in the tropics // Journal Geophys. Res., 1990, Vol.95, P.9927-9939.
7. *Lee T.M., Tag P.M.* Improved detection of hotspots using the AVHRR 3.7 μm channel // Bull. Amer. Meteorol. Soc., 1990. Vol.71, P.1722-1730.
8. *Li Z., Nadon S., Chilar J., Stocks B.* Satellite mapping of Canadian boreal forest fires: Evaluation and comparison of algorithms // International Journal of Remote Sensing, 2000, Vol.21, P.3071-3082.
9. *Arino O. et al.* ATSR World Fire Atlas validation. ESA-ESRIN, Italy, 2000.
10. *Justice C.O., Malingreau J.P.* (editors). The IGBP satellite fire detection algorithm workshop technical report, IGBP-DIS Working paper 9, NASA/GSFC, Greenbelt, Maryland, USA, February, 1993.
11. *Kaufman Y.J., Justice C., Flyn L., Kendall J., Prins E., Ward D.E., Menzel P., Setzer A.* Potential global fire monitoring from EOS-MODIS // Journal of Geophys. Res., 1998, Vol.103, P.32215-32238.
12. *Giglio L., Kendall J.D.* Application of the Dozier retrieval to wildfire characterization. A sensitivity analysis // Remote Sensing of Environment, 2001, Vol.77, P.34-49.

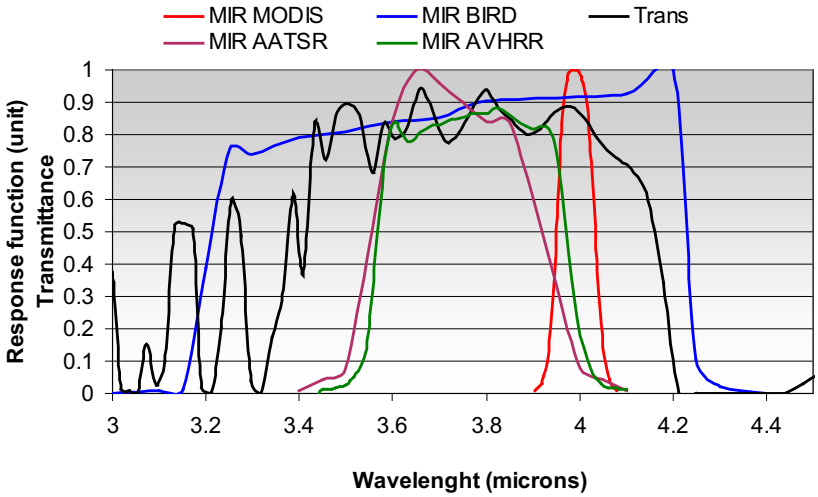

Fig.1. Comparison between different MIR spectral response functions: AVHRR, BIRD, MODIS & AATSR.

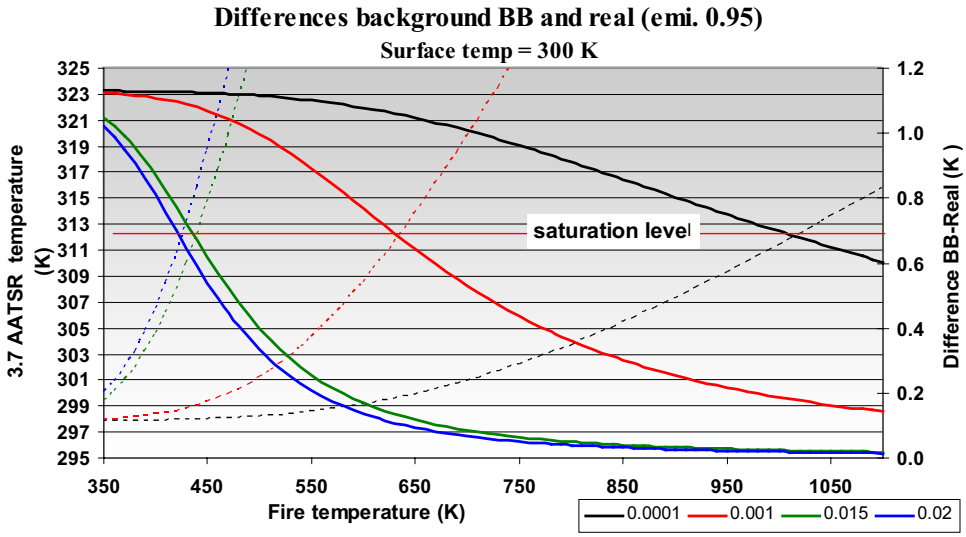

Fig.2. Effect of the considering different surface emissivity values over brightness temperature in AATSR-MIR channel. Different fire fraction of pixel are considered too.

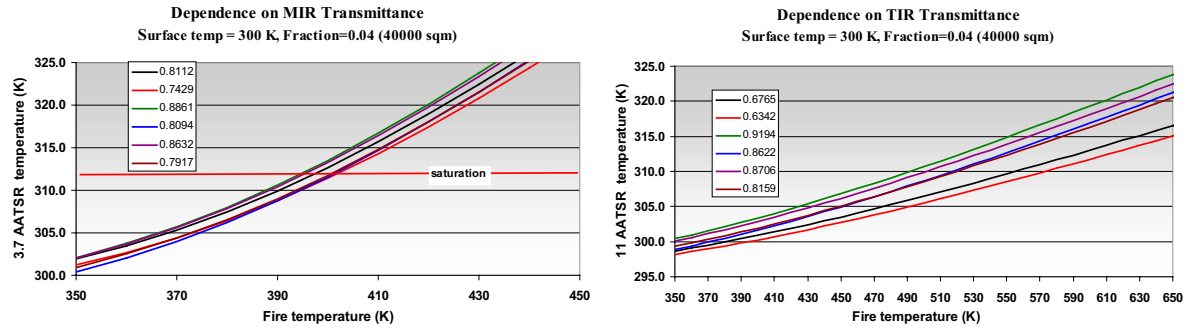

Fig.3. MIR temperature values for different transmittances and different fire temperature.

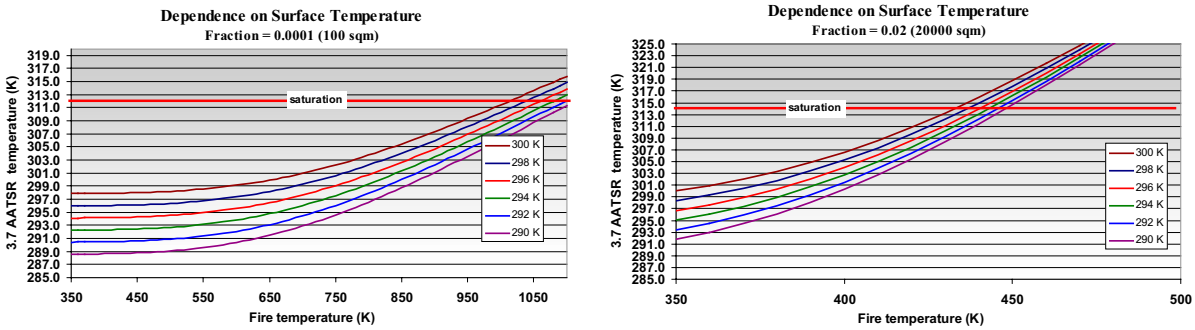

Fig.4. MIR temperature values for different surface temperature and different fire temperature.

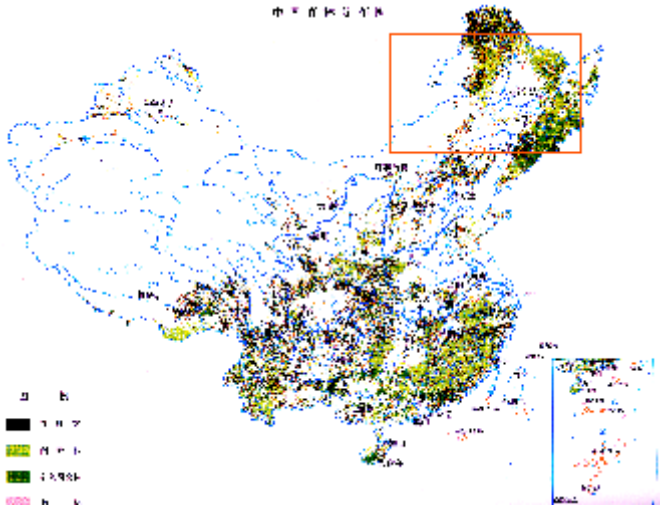

Fig.5. Forest cover analyzed in China

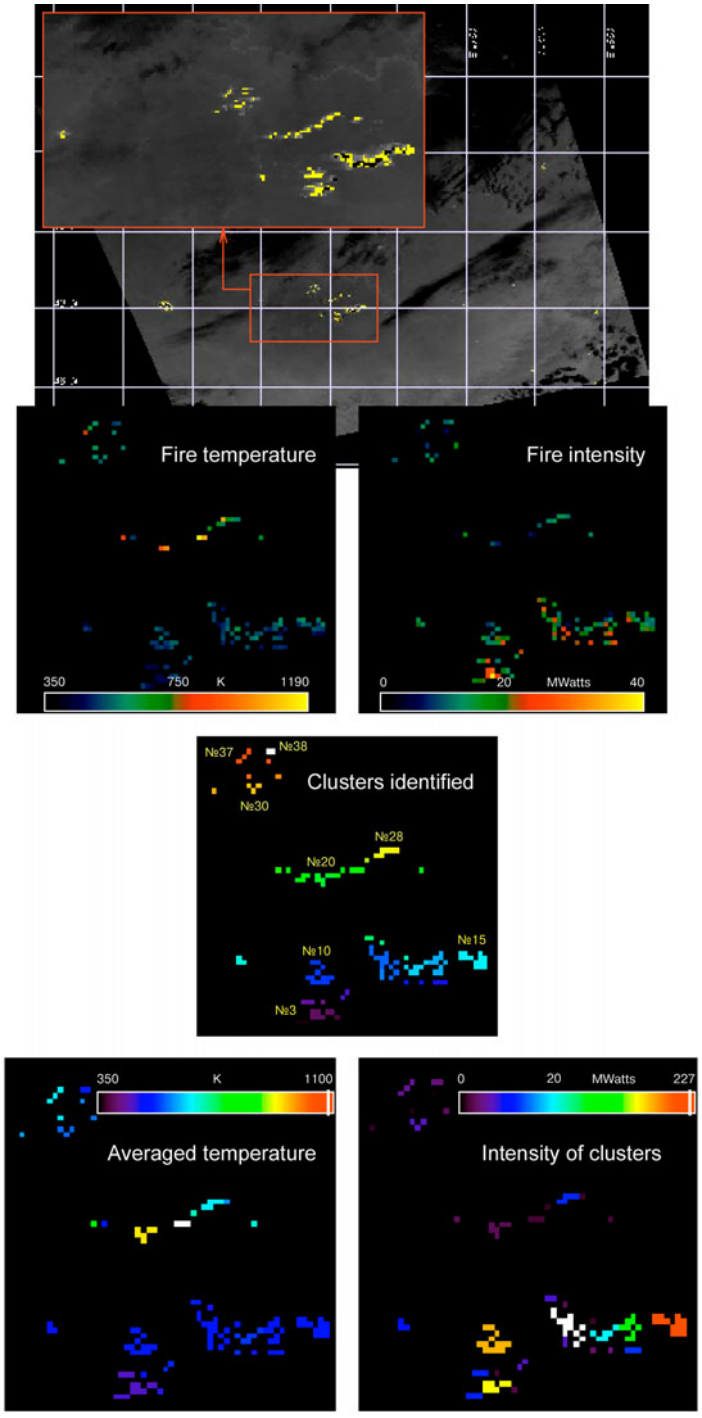

Fig.6. Fire monitoring result.